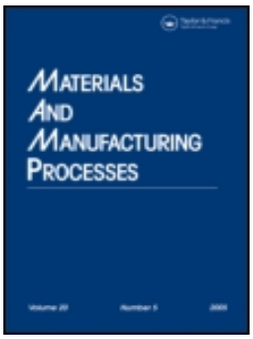

Materials and Manufacturing Processes

ISSN: 1042-6914 (Print) 1532-2475 (Online) Journal homepage: www.tandfonline.com/journals/lmmp20

Modeling Aspects of Hot Densification and Deformation Studies on Al–TiB_2 Composite Preforms

Md. Ahasan & M. J. Davidson

To cite this article: Md. Ahasan & M. J. Davidson (2015) Modeling Aspects of Hot Densification and Deformation Studies on Al–TiB_2 Composite Preforms, Materials and Manufacturing Processes, 30:10, 1190-1195, DOI: 10.1080/10426914.2015.1019099

To link to this article: https://doi.org/10.1080/10426914.2015.1019099

Materials and Manufacturing Processes, 30: 1190–1195, 2015

ISSN: 1042-6914 print/1532-2475 online
DOI: 10.1080/10426914.2015.1019099

Taylor & Francis
Taylor & Francis Group

Modeling Aspects of Hot Densification and Deformation Studies on Al–TiB_2 Composite Preforms

Md. Ahasan and M. J. Davidson

Mechanical Engineering Department, National Institute of Technology, Warangal, India

The modeling aspects of hot deformation and densification behavior of Al–TiB_2 composites are discussed in the present paper. A constitutive relation capable of relating the flow stress to the strain at different temperatures, namely 200°C, 300°C, 400°C, and 500°C, and at different strain rates, namely 0.12, 0.14, 0.16, and 0.18 s^{-1}, have been developed and the developed relation has been used to predict the deformation behavior and the densification attained for different deformation levels and temperatures. The distribution of density and the location of maximum and minimum density zones have been predicted using DEFORM 2D, a finite element analysis (FEA) based software. The damage mechanism that governs the densification process has been identified and the critical damage value has been found.

Keywords Al–TiB_2 sintered preforms; Constitutive equation; Damage; DEFORM-2D; FEA; Hot deformation; Hot densification; Modeling; P/M.

Introduction

The composites of aluminum with different proportions of TiB_2 are used in applications where high temperature stability is required. The properties such as low density, high strength to weight ratio, high stiffness, and high strength at elevated temperature make these composites highly suitable for high temperature applications. The present paper deals with the application of finite element based simulation studies to analyze the densification and deformation behavior of Al–TiB_2 composites. The mechanical and metallurgical properties of the composite developed are required for implementing the simulation strategies. However, due to the presence of pores in the powder metallurgical (P/M) products, the densification and deformation behavior are different from the conventional fully dense material. The presence of pores and the closing of the pores by the upsetting mechanism make density variations across the domain of the preforms and this makes it difficult to predict the variation in property of these P/M products. Thus, the study on densification and deformation mechanism of P/M products is an active research area in the international arena. Mohan Raj et al. [1] performed experimental investigations to study the deformation and densification behavior during cold upsetting of Fe–C–Mn composite preforms. The authors found the preforms with higher manganese content to exhibit better compaction and load-bearing capacity compared to lower manganese preforms. Sumathi et al. [2] studied the workability behavior of cold upsetting of Cu–SiC powder preforms. Rajeshkannan et al. [3] performed deformation studies on iron–carbon–silicon–copper steel compacts and found that copper content and frictional conditions influenced the deformation conditions of the composites considerably. Jayakumar et al. [4] have synthesized A356-Sic_p composite through vacuum hot pressing route. Analyzing the upsetting process using finite element techniques is one useful method which can aid the users to visualize the process of densification and to understand the process better. Though the experimental investigations are plenty, modeling studies on P/M densification behavior are very limited. Chandrasekar et al. [5] have investigated the dynamic effects of cold upsetting of sintered aluminum truncated conical preforms. The authors have used DEFORM 3D to model the process and have used statistical techniques such as response surface method and design of experiments to predict the response and to optimize it. Zhang et al. [6] simulated and predicted the fracture for sintered materials in upsetting using finite element analysis (FEA) method. The authors studied the distribution of density, strain, and stress on the preforms upset to 50% height reduction. The authors were able to establish the formability limits of aluminum 601 AB alloy for different initial preform and aspect ratio conditions. Huang et al. [7] performed simulation studies on the forging of sintered powder compacts under different frictional conditions. ABAQUS software was used for the upsetting process. A gear blank was forged by the authors and the study revealed that the voids present were the primary reason for the degradation of strength of the metal. Lin et al. [8] performed FEA studies to analyze skin-pass axisymmetric drawing process to investigate the inhomogeneous deformation and residual effect on the process. Kandavel et al. [9] have optimized the

Received September 19, 2014; Accepted January 15, 2015

Address correspondence to Md. Ahasan, Mechanical Engineering Department, National Institute of Technology, Warangal, India; E-mail: mdahasankhan@gmail.com.

Color versions of one or more of the figures in the article can be found online at www.tandfonline.com/lmmp.

deformation and densification properties of the sintered plain carbon steel preforms. The authors used Taguchi–Grey relation technique to optimize the parameters such as aspect ratio and load for maximum deformation and density. Though few work have been performed on the modeling aspects of cold and hot upsetting of Al alloys, the studies on the densification and deformation characteristic of Al–TiB_2 and the subsequent modeling studies are limited.

In the present study, the modeling aspects of the sintered P/M upsetting process have been studied and the various aspects such as metal flow path, strain attained, distribution of density, its levels at various deformation zones etc. have been studied. DEFORM 2D software has been used and the process has been modeled by incorporating a constitutive relation that relates the flow stress with strain for various deformation temperatures and strain rates.

Materials and methods

Aluminum (Al) powder of particle size 46 μm was obtained from SRL laboratories Mumbai, India. Titanium diboride (TiB_2) powder was obtained from Alfa Aesar, a Johnson Mathey Company, Hyderabad, India. The SEM images of pure aluminum and titanium diboride powders are shown in Fig. 1(a) and (b), respectively. The aluminum powder and TiB_2 were partially oxidized. Desired quantity of the powders of Al and TiB_2 were weighed and blended using a porcelain bowl by stirring manually. The blended Al–5%TiB_2 composites were poured into a die of size 15 mm diameter and 30 mm height and the walls of the die was coated with zinc stearate. The preforms were made with aspect ratio of 0.75 on a hydraulic press of 0.5 MN capacity, under required pressure to obtain different initial preform densities (IPD), namely initial preform density 0.80, 0.85, and 0.90. The compacts were sintered at a temperature of 550°C for 1 h in a tubular furnace under controlled atmosphere. The sintered preforms were pressed again in a hydraulic press of 50 ton capacity incrementally to different height reductions. Gradual increase of load was applied to each billet up to the initiation of crack on the free surface. The top contact diameter (D_{top}), the bottom contact diameter (D_{bottom}), the bulge diameter (D_b), and the final height (H_f) were noted by using digital vernier calliper and the density was measured by using Archimedes' principle for each of the deformed compacts before and after each step of deformation.

In hot compression of metallic material, the relationship between the flow stress of the material and deformation parameters, such as the deformation temperature and strain rate can be expressed as [10]

$$z = \dot{\varepsilon}\exp\left(\frac{Q}{RT}\right) = F(\sigma) \tag{1}$$

$$\dot{\varepsilon} = Z\exp\left(-\frac{Q}{RT}\right) = F(\sigma)\exp\left(-\frac{Q}{RT}\right) \tag{2}$$

where Z (Zener–Hollomon parameter) is the deformation corrected strain rate, $\dot{\varepsilon}$ is the strain rate (s^{-1}), Q is the activation energy of hot deformation (J/mol), R is the gas constant (8.31 $Jmol^{-1}K^{-1}$), and T is the absolute temperature (K). $F(\sigma)$ is called the stress function and corresponds to one of the following equations depending on the deformation conditions:

$$F(\sigma) = A_1\sigma^n = Z \tag{3}$$

$$F(\sigma) = A_2\exp(\beta\sigma) = Z \tag{4}$$

$$F(\sigma) = A_3[\sinh(\alpha\sigma)]^n = Z \tag{5}$$

Equation (3) is used in the applications where low stress levels are involved, whereas Eq. (4) is used where higher levels of stress and strain rates are involved. Equation (5) can be used for both low and high stress and strain levels [11]. In the above equations, A_1, A_2, A_3, α, and β are material constants.

Flow curves of the compacts at different deformation temperatures and initial preform densities were drawn to develop the constitutive relation. The true stress and true strain of the composites at various temperatures and strain rates were determined by performing series of hot compression tests.

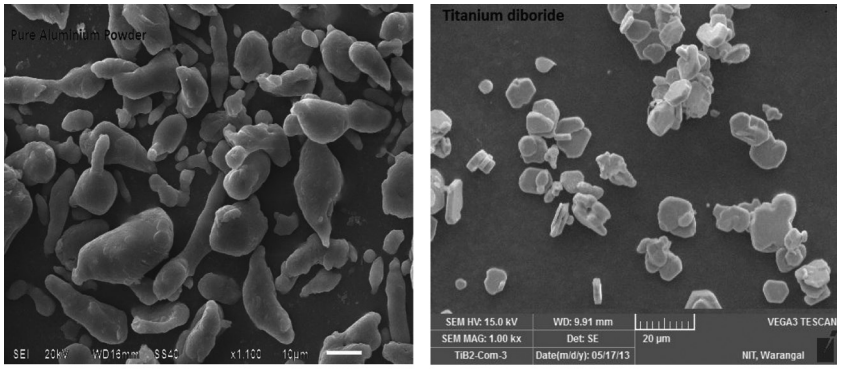

(a) (b)

Figure 1.—(a) SEM images of pure aluminum. (b) SEM image of titanium diboride (TiB_2).

Figure 2(a–d) show a sample true stress–strain curve for Al–TiB_2 composites for different initial preforms densities and strain rates at 200°C. Similarly, flow curves were drawn for 300°C, 400°C, and 500°C. Almost all the curves showed two zones of deformation. In Zone 1, the stress increased drastically during the initial stage of the deformation up to a critical strain region followed by a region of flat zone (Zone 2). In some cases, a small decrease in true stress was witnessed after the critical stress due to dynamic recrystallization effect. Such behavior was predominant in the preforms with 80% IPD. This phenomenon was witnessed at higher strain region for the preforms with 85% and 90% IPD.

DEFORM 2D uses a relation given in Eq. (6) to relate the stress and strains:

$$\dot{\varepsilon} = A[\sinh \alpha \sigma]^n \exp\left[-\frac{Q}{RT}\right] \tag{6}$$

$$\ln A = \ln \dot{\varepsilon} + \frac{Q}{RT} - \beta\sigma \tag{7}$$

The material constants such as A, α, β, Q, and n can be found from the experimental data collected from the hot compression tests. The value A can be found from Eq. (7), in which, $\dot{\varepsilon}$ is the strain rate and Q is the activation energy. The slope of the graph drawn between ln sinh($\alpha\sigma$) and 1/T gives Q/Rn, from which the value of Q can be evaluated by multiplying the value with strain hardening index, n and the gas constant, R. The value for β is found from the graph drawn between ln $\dot{\varepsilon}$ and true stress (σ). The value for α is found from the relation β/n_1, where n_1 can be found from the graph drawn between ln $\dot{\varepsilon}$ and ln stress (σ). A sample graph used to find the value for β is shown in Fig. 3. Similarly, other constants were evaluated and the values thus evaluated are given in Table 1. The detailed procedure for developing the constitutive relation for P/M preforms has been explained by Desalegn Wogaso et al. [11].

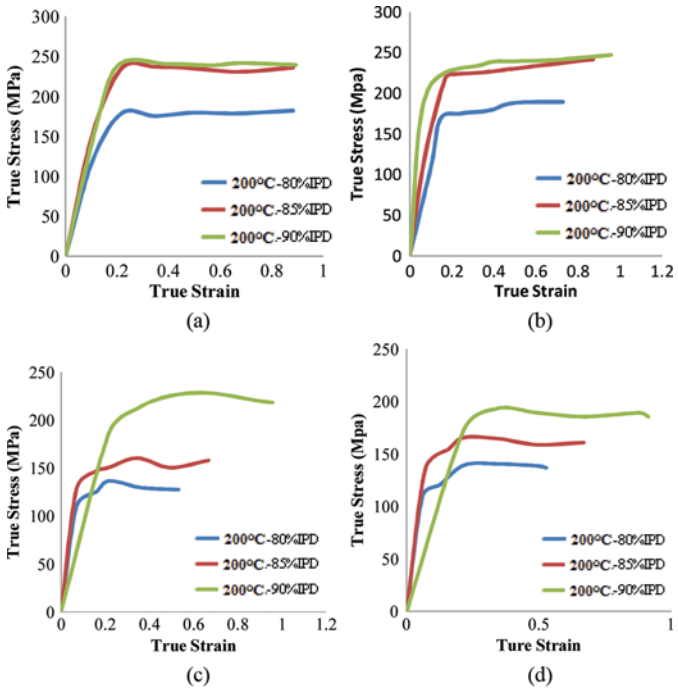

FIGURE 2.—True stress–true strain curves of sintered Al–5%TiB_2 powder compacts hot compressed at 200°C and at different strain rates of (a) 0.12 s^{-1}, (b) 0.14 s^{-1}, (c) 0.16 s^{-1}, and (d) 0.18 s^{-1}.

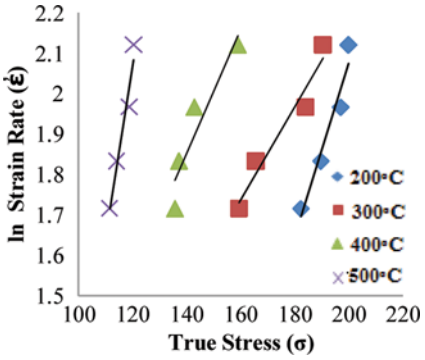

FIGURE 3.—Relationship between ln strain rate ($\dot{\varepsilon}$) and true stress for 80% IPD at different temperatures.

The values thus calculated for different initial preform densities were drawn into curves as shown in Fig. 4 and the statistical equations developed from the curves for each material constants are given below:

$$Z = \dot{\varepsilon} \exp\left(\frac{Q}{RT}\right) = A \exp(\beta\sigma)$$

$$\beta = -0.2408(RD)^2 + 0.335(RD) - 0.1045$$

$$\ln(A) = y = 336x^2 - 543.6x + 227.48$$

$$Q = -765308(RD)^2 + 1E + 06(RD) - 601067$$

The DEFORM 2D simulations performed must have a limiting criteria to let the user know the limits to which the simulations are valid. In the present work, Cockcroft Lantham algorithm has been used as a limiting criterion. The algorithm is stated as below:

$$\int_0^{\bar{\varepsilon}} \frac{\sigma^*}{\bar{\sigma}} d\bar{\varepsilon} = c \tag{8}$$

where σ^* is the maximum tensile stress, $\bar{\sigma}$ the effective stress, and $\bar{\varepsilon}$ the equivalent strain The peak value of

TABLE 1.—The material constants "A," "α," "n," and "Q" for powder compacts with different IPD.

IPD	A	α	n	Q (Jmol^{-1})	β	ln A
80%	2079.74	0.009362	2.08	28708.19	0.02865	7.64
85%	3568.85	0.01929	7.80	35543.53	0.02405	8.18
90%	32859.62	0.06248	2.52	38552.33	0.02285	10.40

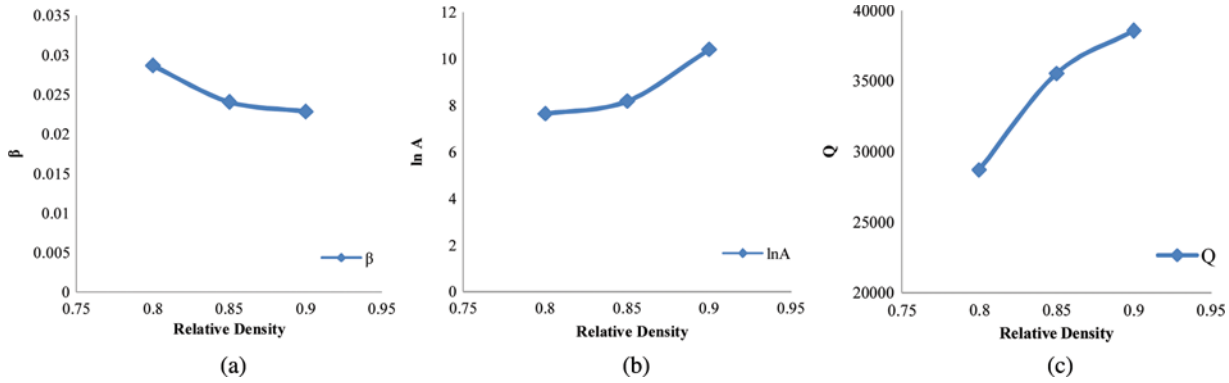

FIGURE 4.—(a–c). Relationship between the relative density of powder compact and β, ln A, and Q.

the damage factor is known as critical damage factor. The critical damage factor for various powder compacts at various temperatures and initial preform conditions are given in Table 2.

RESULTS AND DISCUSSION

Simulations were performed with preforms of different initial preform densities and at different forming temperatures. The failure strain and the final density attained were critically analyzed. It was found that the preforms with IPD of 80% showed very less uniform strain region and failed at strains of 0.5 and 0.59 when deformed at 300°C and 400°C, respectively. The formability improved when deformed at 500°C and the compacts failed at a strain of 0.71. The maximum densification attained was 0.92% and much variation could not be found between the preforms deformed at different temperatures as it is evident from Table 3. The metal flow path and the regions of density progression were studied through simulations and it was found that the densification started initially at the middle and at the corners of the preforms as a spherical ball and it progressed to the whole domain of the compacts in a double cross profile till it filled the whole domain. The distribution of density for an 80% IPD preform at 300°C is shown in Fig. 5.

As the material flow intensity is more in the center of the compact and the progression of the metal is from the center to the edge, the densification is found to be more in the center than at the edge. However, at the end of the upsetting cycle, before the failure, a more or less uniform densification was achieved throughout the compact. The material flow path of the preform is shown in Fig. 6.

Table 4 shows the effect of forming temperature on the densification and deformation behavior during the simulation studies. It was observed that the densification attained was more at higher forming temperature for the preforms with 80% IPD. The maximum density attained was more or less same for the different samples deformed at different temperatures. However, the strain path was different for different forming temperatures. The strain path is a measure of the level of work

TABLE 2.—Critical damage factors for different IPD at different forming temperatures.

Initial preform density	Forming temperature (°C)	Critical damage factor
80%	300	0.070
	400	0.091
	500	0.115
85%	300	0.142
	400	0.148
	500	0.141
90%	300	0.290
	400	0.287
	500	0.248

TABLE 3.—The values of failure strain and final density for different IPD at different forming temperatures.

Initial preform density	Forming temperature (°C)	Failure strain	Final density
80%	300	0.50	0.90
	400	0.59	0.91
	500	0.71	0.92
85%	300	0.82	0.93
	400	0.84	0.94
	500	0.85	0.96
90%	300	0.92	0.94
	400	0.91	0.95
	500	0.84	0.96

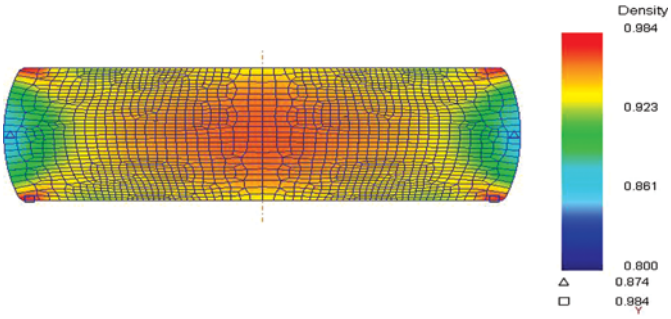

FIGURE 5.—Density propagation at 300°C for 80% IPD.

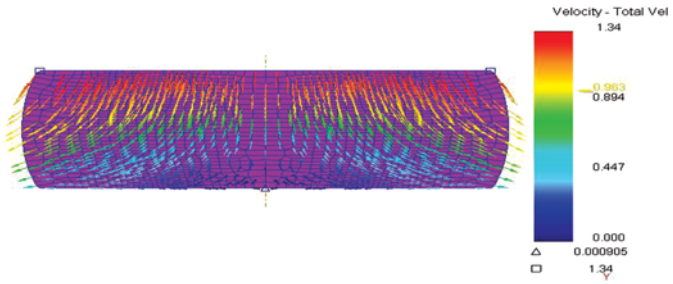

FIGURE 6.—Metal flow behavior during the deformation.

TABLE 4.–The values of failure strain and final density for different temperatures at different IPD.

Forming temperature (°C)	Initial preform density	Failure strain	Final density
300	80%	0.50	0.90
	85%	0.82	0.93
	90%	0.92	0.94
400	80%	0.59	0.91
	85%	0.84	0.94
	90%	0.91	0.95
500	80%	0.71	0.92
	85%	0.85	0.96
	90%	0.84	0.96

hardening attained by the samples. A 80% IPD sample deformed at 300°C had a peak stress of 80 MPa and it failed at a strain of 0.5 whereas a 90% IPD preform shows a strain path with more uniform strain region and with a peak stress of 160 MPa and a failure strain of 0.92. However, at higher temperatures, though the densification attained was almost same, the strain path differed resulting in different strength levels. From Fig. 7 it is evident that the peak stress attained by the preform with lower initial preform density is more than that of the preforms with higher initial preform densities. This is due to the higher work hardening that has taken place in a low IPD preform.

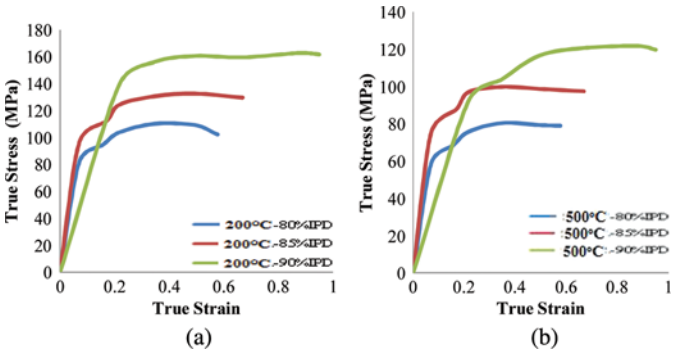

FIGURE 7.—(a–b) True stress–true strain curves of sintered Al–5%TiB_2 powder compacts hot compressed at (a) 300°C and (b) 500°C at strain rate 0.12 s^{-1}.

CONCLUSIONS

The densification and deformation mechanism of P/M Al–TiB_2 composites have been studied through modeling route and the material properties required for modeling have been developed. The constitutive relation that has been developed was found to predict the deformation within acceptable error range. The simulation study performed enabled the investigators to predict the material flow path, densification attained, and the failure strain. The damage criteria developed through Cockcroft–Lantham algorithm predicted the damage zone accurately. The simulation methodology proposed through this paper and the various high temperature material properties that have developed for the simulation study can be used by any user of this composite to perform forming studies through simulation mode.

FUNDING

The investigators would like to thank CSIR, India, for funding the work through a project grant no: 22(0650)/13/EMR-II with the title "Modelling studies on the hot deformation and densification behavior of sintered Al–TiB_2 composites and its tribological characterization" to Dr M J Davidson.

REFERENCES

1. Mohan Raj, A.P.; Selvakumar, N. Deformation behavior of sintered Fe-C-Mn composite during cold upset forming. *Materials and Manufacturing Processes* **2011**, *26* (11), 1388–1392. DOI: 10.1080/10426914.2010.544820
2. Sumathi, M.; Selvakumar, N. Phenomenon of workability behaviour of Cu-SiC sintered preforms during cold upsetting. *Materials and Manufacturing Processes* **2011**, DOI:10.1080/10426914.2011.593233
3. Rajeshkannan, A.; Utkal, Mehta. Deformation study of sintered iron–carbon–silicon–copper steel compacts during cold forging. *Materials and Manufacturing Processes* **2014**, *29* (4), 442–447. DOI:10.1080/10426914.2013.864401
4. Jayakumar, K.; Jose, Mathew; Joseph, M.A.; Suresh Kumar, R.; Shukla, A.K.; Samuel, M.G. Synthesis and characterization of A356-Sic_p composite produced through vacuum hot pressing. *Materials and Manufacturing Processes* **2013**, *28* (9), 991–998. DOI: 10.1080/10426914.2013.773012
5. Chandrasekhar, P.; Singh, S. Investigation of dynamic effects during cold upset-forging of sintered aluminium truncated conical preforms. *Journal of Material Processing Technology* **2011**, *211*, 1285–1295. DOI: 10.1016/j.jmatprotec.2011.02.010
6. Zhang, X.Q.; Peng, Y.H.; Ruan, X.Y. Simulation and fracture prediction for sintered materials in upsetting by FEM. *Journal of Material Processing Technology* **2000**, *105* (3), 253–257. DOI: 10.1016/S0924–0136(00)00560–4
7. Cheng-Chao, Huang; Jung-Ho, Cheng. Forging simulation of sintered powder compacts under various frictional conditions. *International Journal of Mechanical Sciences* **2002**, *44* (3), 489–507. DOI: 10.1016/S0020–7403(01)00107–2
8. Heng-Sheng, Lin; Yuan-Chuan, Hsu; Chia-Chow, Keh. Inhomogeneous deformation and residual stress in skin-pass axisymmetric drawing. *Journal of Material Processing*

Technology **2008**, *201*, 128–132. DOI: 10.1016/j.jmatprotec.2007.11.126

9. Kandavel, T.K.; Panneerselvam, T.; Karthikeyan, P. Optimization of deformation and densification properties of the sintered plain carbon steel. *Materials and Manufacturing Processes* **2014**, DOI: 10.1080/10426914.2013.840908 (In Press)
10. Zener, C.; Hollomon, J.H. Effect of strain rate upon plastic flow of Steel. *Journal of Applied Physics* **1944**, *15*, 22–32.
11. Desalegn Wogaso, W.; Davidson, M.J.; Asit Kumar, Khanra. Constitutive modeling of powder metallurgy processed Al-4%Cu preforms during compression at elevated temperature. *Materials and Design* **2015**, *65*, 83–93. DOI: 10.1016/j.matdes.2014.08.069